Desalination and Water Treatment
www.deswater.com

doi: 10.5004/dwt.2019.24300

162 (2019) 260–268
September

Dichlorocarbene modified graphene oxide nanocomposite fabricated by a facile hydrothermal method and its adsorption properties toward rare earth elements

Jia-Ying Yang[a], Bao-Yu Yue[a], Jie-Teng[b,*], Qi Liu[a,*], Xin-Yu Jiang[a], Ming Zhong[c,*], Fang-Liang Zhou[d], Jin-Gang Yu[a,*]

[a]*College of Chemistry and Chemical Engineering, Key Laboratory of Hunan Province for Water Environment and Agriculture Product Safety, Central South University, Changsha, Hunan 410083, China, Tel./Fax: +86-731-88879616; emails: iliuqi@csu.edu.cn (Q. Liu), yujg@csu.edu.cn (J.-G. Yu), 919620862@qq.com (J.-Y. Yang), 775498809@qq.com (B.-Y. Yue), jiangxinyu@csu.edu.cn (X.-Y. Jiang)*
[b]*College of Materials Science and Engineering, Hunan University, Changsha, Hunan 410082, China, Tel./Fax: +86-731-88821610; email: tengjie@hnu.edu.cn*
[c]*School of Chemistry and Chemical Engineering, Hunan Institute of Science and Technology, Yueyang, Hunan 414006, China, email: zhongming2613@163.com*
[d]*Hunan Vocational College of Engineering, Changsha, Hunan 410151, China, email: yjgzfl@126.com*

Received 13 January 2019; Accepted 19 April 2019

ABSTRACT

Dichlorocarbene modified graphene oxide (GO-CCl_2) was prepared via a facile hydrothermal method by using GO as the substrate material. The morphology and chemical compositions of the as-prepared material were characterized by Fourier transform infrared (FT-IR) spectroscopy, Raman spectroscopy, thermogravimetric analysis and field emission scanning electron microscopy (FE-SEM). Additionally, the material was used to adsorb five kinds of rare earth elements (REEs), including La(III), Y(III), Yb(III), Er(III) and Nd(III) from aqueous solutions, and the adsorption kinetics and thermodynamics of GO-CCl_2 for Yb(III) were investigated in detail. The GO-CCl_2 was also applied to remove REEs from real water samples including spring water, Xiangjiang River, Yudai River and tap water, and the results showed that GO-CCl_2 owned relatively high stability and satisfactory adsorption capacity in complicated natural water system, and the highest removal rates reached to 100% for La(III) and >90% for other REEs in tap water. Therefore, it is proposed that GO-CCl_2 can be used to remove REEs from aqueous solutions.

Keywords: Graphene oxide; Dichlorocarbene; Rare earth elements; Adsorption; Hydrothermal assisted synthesis

1. Introduction

Rare earth elements (REEs) are widely distributed in the earth's crust, which have played a crucial role in many application fields, including catalysis, hydrogen storage, luminescence, magnetic ceramics and so on [1]. Owing to the high demand and consumption for REEs in various industries, the exploitation methods were continuously improved and optimized. The total global reserves of REEs represented a dramatic decrease in the past decades due to the excessive exploration to meet the needs of economic and scientific development, which has eventually attracted great attention from the government [2,3]. During mining, smelting and separating procedures, it is very likely to discharge REEs into soil, air and water. It is worth noting that REEs distributions in some rocks and associated minerals have

* Corresponding author.

been discharged into water systems and contributed a lot to water pollution [4]. However, even trace amount of REEs in the environment would cause serious consequences for animal and human health. For example, trace Gd(III) ion may result in abnormal proliferation of cervical carcinoma cells-HeLa cells in human body [5]. Hence, the maximum degree of REEs in wastewater should be controlled. And the recovery of REEs also becomes necessary due to the constantly escalating future needs of such crucial and limited natural resourcesg. The discharged REEs can be regenerated from contaminated water, and the environmental pollution would also be reduced. Despite several separation and enrichment methods such as precipitation, solvent extraction, ion exchange, liquid membrane extraction and so on, adsorption still counts for a lot for the recovery REEs [6–9]. Traditional adsorbents including activated carbon, by-pass cement dust, γ-Al_2O_3, bacterial cell walls and clay minerals, have been applied in the adsorption of REEs in the past [10–13]. However, the development of efficient, promising and feasible adsorbents for the recycling of REEs was still a challenge [14].

As an emerging and potential nanomaterial, graphene was discovered and characterized in 2004 by Novoselov et al. [16], which has attracted much attention by many scholars in recent years [15,17–20]. Due to the hexagonal lattice structure of graphene alignment, graphene-based materials displayed many special properties such as superior electron mobility, thermal conductivity, excellent optical and mechanical properties [21–25]. One of the graphene derivatives, graphene oxide (GO), possesses plentiful oxygen-rich functional groups containing epoxy, hydroxyl and carboxyl groups which provide a large number of binding sites [26–29]. GO is also highly hydrophilic and could be homogeneously dispersed in water [30–32]. The large theoretical surface area of GO is beneficial when it is fully contact with targeted adsorbates such as dyes, heavy metal ions, REEs and phenols. However, the lack of other functional groups, especially hydrophobic groups, would generate strong inter planar interaction among GO layers and affect the whole adsorption efficiency [33]. Up to now, many research studies on GO composites have been implemented, indicating that appropriate modifications of GO can overcome the above-mentioned shortcomings [34–37]. For instance, a porous hydrogel nanocomposite composed of chitosan-poly(acrylic acid) (CS-PAA) and GO showed satisfactory lead ions (Pb(II)) removal [38], and nitrogen-containing amino (NA) modified GO showed selective adsorption capability for copper ions (Cu(II)) and Pb(II) [39]. The preparation and application of dihalocarbenes including dichlorocarbene (–CCl_2), dibromocarbene (–CBr_2) and diiodocarbene (–CI_2) modified carbon nanomaterials seems to be feasible. For example, –CI_2 modified reduced multiple-walled carbon nanotubes (MWCNTs-CI_2) showed satisfactory adsorption ability toward Pb(II) than as-received MWCNTs due to the additional coordination interactions between –I and Pb(II) [40]. And –CBr_2 functionalized reduced GO (RGO-CBr_2) possessed much higher adsorption capacities toward Pb(II) than that of as-received RGO, indicating that the coordination interactions between halogen atoms and metal ions are beneficial to the highly efficient adsorption of metal ions [41]. Additionally, the oxygen-containing groups are also helpful for increasing the equilibrium adsorption capacity of an adsorbent [42].

To achieve more efficient aqueous adsorption of REEs, dichlorocarbene modified GO (GO-CCl_2) nanocomposite was fabricated through a facile hydrothermal method (Fig. 1), and its adsorption properties were evaluated. To the best of our knowledge, this is the first attempt for attaching dichlorocarbene onto GO by a facile hydrothermal method. The newly developed graphene-based adsorbent possessed both abundant oxygen-containing and halogen groups, and its application on adsorption of REEs from aqueous solutions was evaluated and discussed.

2. Experimental details

2.1. Materials

Flake graphite as a raw material was supplied by Tianjin Kermel Chemical Reagent Development Center (Tianjin, China) with higher purity of >99.85%. And potassium permanganate ($KMnO_4$), phosphoric acid (H_3PO_4), sulfuric acid (H_2SO_4), hydrochloric acid (HCl), benzyl triethyl ammonium chloride (TEBA) and hydrogen peroxide (H_2O_2) were all obtained from Sinopharm Chemical Reagent Beijing Co., Ltd. (Shanghai, China). Chloroform ($CHCl_3$) was bought from Tianjin Zhiyuan Chemical Reagent Co., Ltd. (Tianjin, China). All reagents were of analytical grade and used with no further purification. Ytterbium chloride hexahydrate

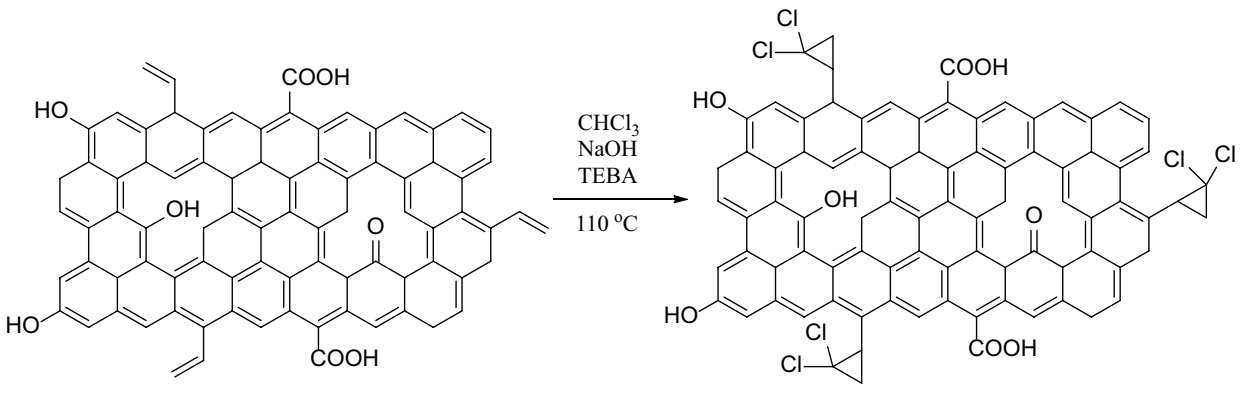

Fig. 1. Synthesis of GO-CCl_2.

($YbCl_3·6H_2O$; 99.99 wt.%), lanthanum chloride heptahydrate ($LaCl_3·7H_2O$; 9.99 wt.%), erbium chloride hexahydrate ($ErCl_3·6H_2O$; 99.90 wt.%), yttrium chloride heptahydrate ($YCl_3·7H_2O$; 99.90 wt.%) and neodymium chloride hexahydrate ($NdCl_3·6H_2O$; 99.90 wt.%) were provided by Aladdin Chemical Co., Ltd. (Shanghai, China). The real water samples were acquired from the district of Changsha, Hunan province, China.

2.2. Characterization methods

The characteristic functional groups of GO-CCl_2 composite were revealed using Fourier transform infrared (FT-IR) spectroscopy in the wavenumber range 400–4,000 cm^{-1} on a Nicolet 6700 FT-IR spectrometer (Thermo Nicolet Corp., Madison, WI) with pure potassium bromide (KBr) as the background. Raman spectra of GO and GO-CCl_2 composite was measured using a LabRAM HR800 micro-Raman spectrometer (JY Inc., Edison, NJ). Thermogravimetric analysis (TGA) was carried out on a SDT Q600 V8.0 Build 95 thermal analyzer apparatus (Netzsch, Germany) at a heating rate of 10°C min^{-1} in argon (Ar) atmosphere. Moreover, the surface morphologies of as-prepared GO-CCl_2 material were investigated by a MIRA3 TESCAN field emission scanning electron microscopy (FE-SEM; TESCAN, Czech Republic).

2.3. Preparation of GO-CCl_2 composite

GO was prepared by improved Hummers' method reported previously [43–45]. A mixture of flake graphite (300 mg) and $KMnO_4$ powder (1.50 g) was added into a round-bottom flask, and a mixed acid of concentrated H_3PO_4 and H_2SO_4 (40 mL; V/V = 9:1) was added dropwise into the reaction. After being stirred at 50°C for 12 h, the mixture was cooled to room temperature and diluted with 40.0 mL of ice water. Then 3.0 mL of H_2O_2 was added until no bubble appeared, and the solution turned bright yellow. Finally, the mixture was rinsed repeatedly with HCl (1 M) and ultrapure water for three times, GO suspension was obtained with a concentration of 5 mg mL^{-1}.

GO dispersion (10 mL), $CHCl_3$ (8 mL) and NaOH solution (1.0 g mL^{-1}, 8 mL) were mixed TEBA (10 mg), which was then was transferred into an autoclave and hydrothermally treated at 110°C for 2 h. After reaction, the excess alkali was neutralized by adding 1 M HCl. The mixture was filtered, rinsed with ethanol and ultrapure water for several times. The solid residue was dispersed in 10 mL of deionized water and freeze-dried to obtain GO-CCl_2 composite (58 mg).

2.4. Adsorption tests

Trivalent REE ion (REE^{3+}) solutions including lanthanum (La^{3+}), yttrium (Y^{3+}), ytterbium (Yb^{3+}), erbium (Er^{3+}) and neodymium (Nd^{3+}) were prepared by dissolving the corresponding chlorides in ultrapure water, respectively. The adsorption behavior of GO-CCl_2 composite toward La^{3+}, Yb^{3+}, Y^{3+}, Er^{3+} and Nd^{3+} was investigated. In the typical batch experiments, 5 mg of the GO-CCl_2 adsorbents were added into 20 mL of above REE^{3+} solutions (40 mg L^{-1}) for a certain time (10–150 min), the residual REE^{3+} concentrations were determined by inductively coupled plasma optical emission spectroscopy (ICP-OES).

Yb^{3+} was selected as a "model" REE^{3+} to study the adsorption isotherms of GO-CCl_2 adsorbent. 5 mg of GO-CCl_2 was dispersed in 20 mL of Yb^{3+} solution (10, 20, 30, 40, 60 and 80 mg L^{-1}), which were then kept in oscillator at 25°C, 35°C and 45°C for 90 min. After adsorption, the remaining Yb^{3+} concentrations were detected by ICP-OES.

The recovery method was adopted to evaluate the adsorption properties of GO-CCl_2 adsorbent toward REE^{3+} in complex water systems including spring water, Xiangjiang River, Yudai River and tap water. By mixing 10.0 mg of GO-CCl_2 composite and 20.0 mL of La^{3+}, Yb^{3+}, Y^{3+}, Er^{3+} and Nd^{3+} solution (20 mg L^{-1}), the removal rates and adsorption capacities of the adsorbent for the five REE^{3+} were studied.

3. Results and discussion

3.1. Characterization

The morphologies of GO and GO-CCl_2 were investigated by FE-SEM (Fig. 2). In comparison with GO (Fig. 2a),

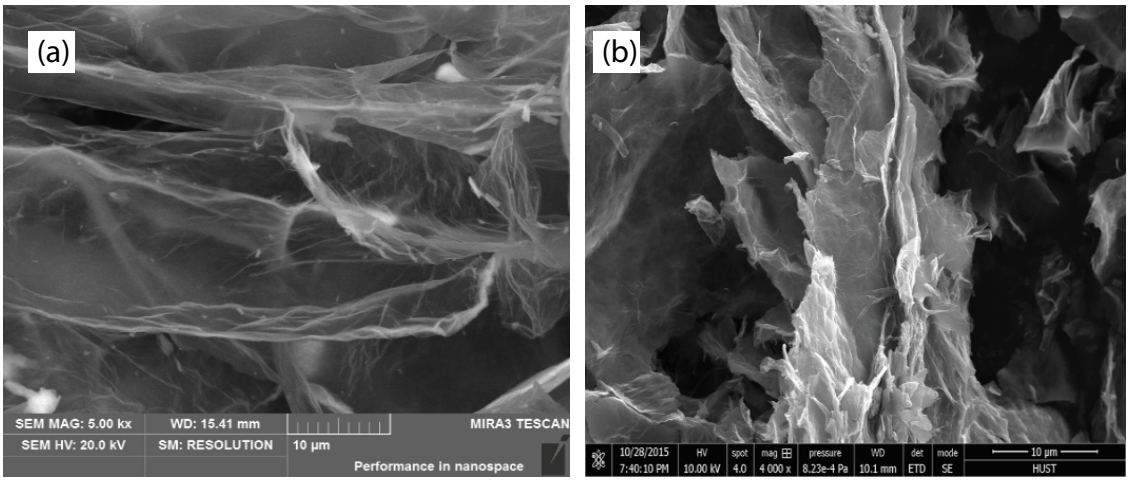

Fig. 2. SEM images of the samples: (a) GO and (b) GO-CCl_2 composite.

more fragment layers and curly edges could be observed for GO-CCl_2, and the layers become rougher (Fig. 2b). Additionally, the GO-CCl_2 layer turns to be a little thicker owing to the increased layer to layer interactions due to the introduced chlorine groups.

Besides SEM characterizations, several typical characterization methods including FT-IR spectroscopy, Raman spectroscopy and TGA were also employed to reveal the structural features of GO-CCl_2 composite. As shown in Fig. 3a, the absorbing peaks of main functional groups, such as O–H group, C–O group and so on, are observed obviously. The peak at 588.11 cm^{-1} could be attributed to the C–Cl group of the prepared composite, demonstrating the attachment of dichlorocarbene onto the surface of GO. Moreover, the C=O peak shifts to the lower wavenumber due to the formed cyclopropane on the graphene sheet.

As for Raman spectra, the D band and G band at 1,350 and 1,580 cm^{-1} are associated with the vibration of sp^3 carbon atom of disorder and defect structure and the sp^2 carbon atom of graphitic hexagonal lattice, respectively. The relative intensity of D band and G band (I_D/I_G) for GO and GO-CCl_2 increased from 0.852 to 1.119, indicating the skeleton structure of graphene sheet was damaged a little due to the attachment of dichlorocarbene (Fig. 3b).

The TGA curve of GO-CCl_2 is displayed in Fig. 3c. A three-step weight loss could be observed in the temperature range 30°C–1,000°C. The first weight loss below 200°C can be assigned to the evaporation of physically adsorbed water in the surface of the GO-CCl_2 composite; the second weight loss of about 18.0 wt.% between 200°C and 400°C might be due to the decomposition of oxygen functional groups; and the third weight loss above 400°C could be attributed to the thermal pyrolysis of cyclopropane structure. Therefore, it can be deduced that dichlorocarbene was successfully grafted onto GO.

3.2. Kinetic studies

The effect of contact time (0–150 min) on the adsorption efficiency of GO-CCl_2 composite for five kinds of REEs (La^{3+}, Yb^{3+}, Y^{3+}, Er^{3+} and Nd^{3+}) was observed by performing experiments at 308 K (Fig. 4a). Obviously, a significant increase in its adsorption capacity during the first 15 min could be observed, and then the adsorption tended to slow down gradually within the next 60 min. The maximum adsorption capacity would be achieved in about 80 min. The adsorption data of GO-CCl_2 composite toward Yb^{3+} were fitted by five kinetic models including pseudo-first-order kinetic model (Eq. (1)), pseudo-second-order kinetic model (Eq. (2)), Elovich model (Eq. (3)), Weber and Morris (W-M) model (Eq. (4)) and Bangham model (Eq. (5)) (Figs. 4b–f). These models are expressed as follows:

$$k_1 t = \frac{\ln q_e}{\ln(q_e - q_t)} \tag{1}$$

$$\frac{1}{q_e} t = \frac{t}{q_t} - \frac{1}{k_2 q_e^2} \tag{2}$$

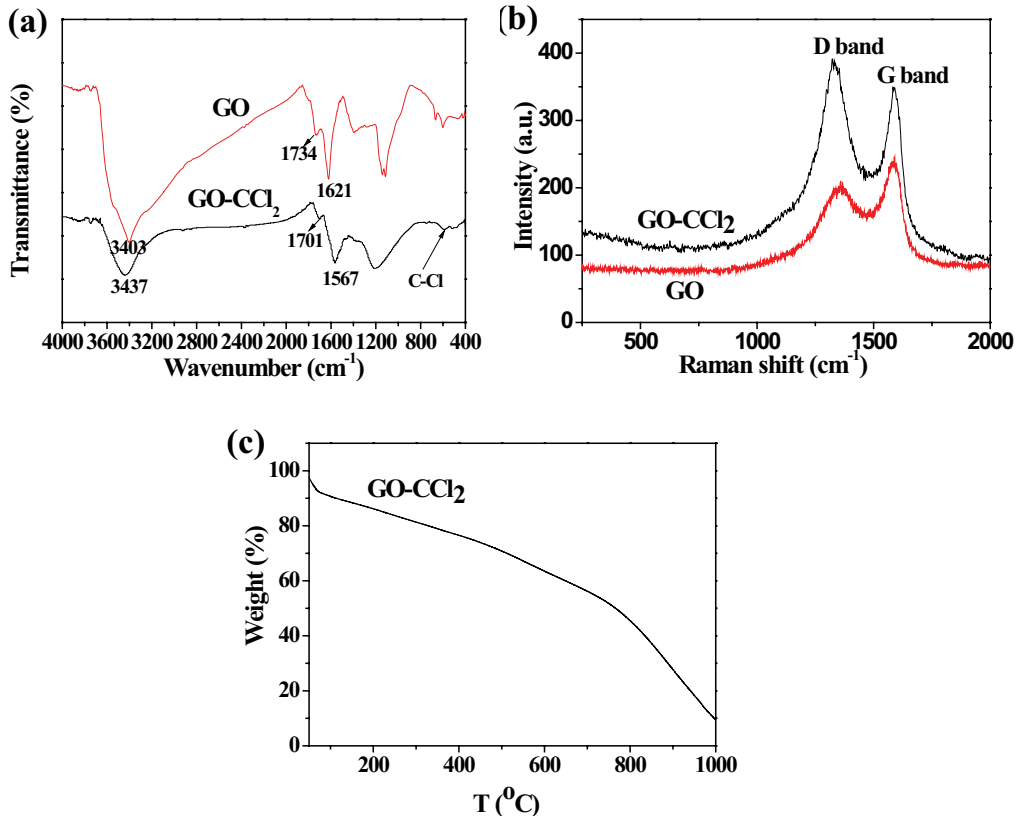

Fig. 3. Characterization of the samples: (a) FT-IR spectra, (b) Raman spectra and (c) TGA.

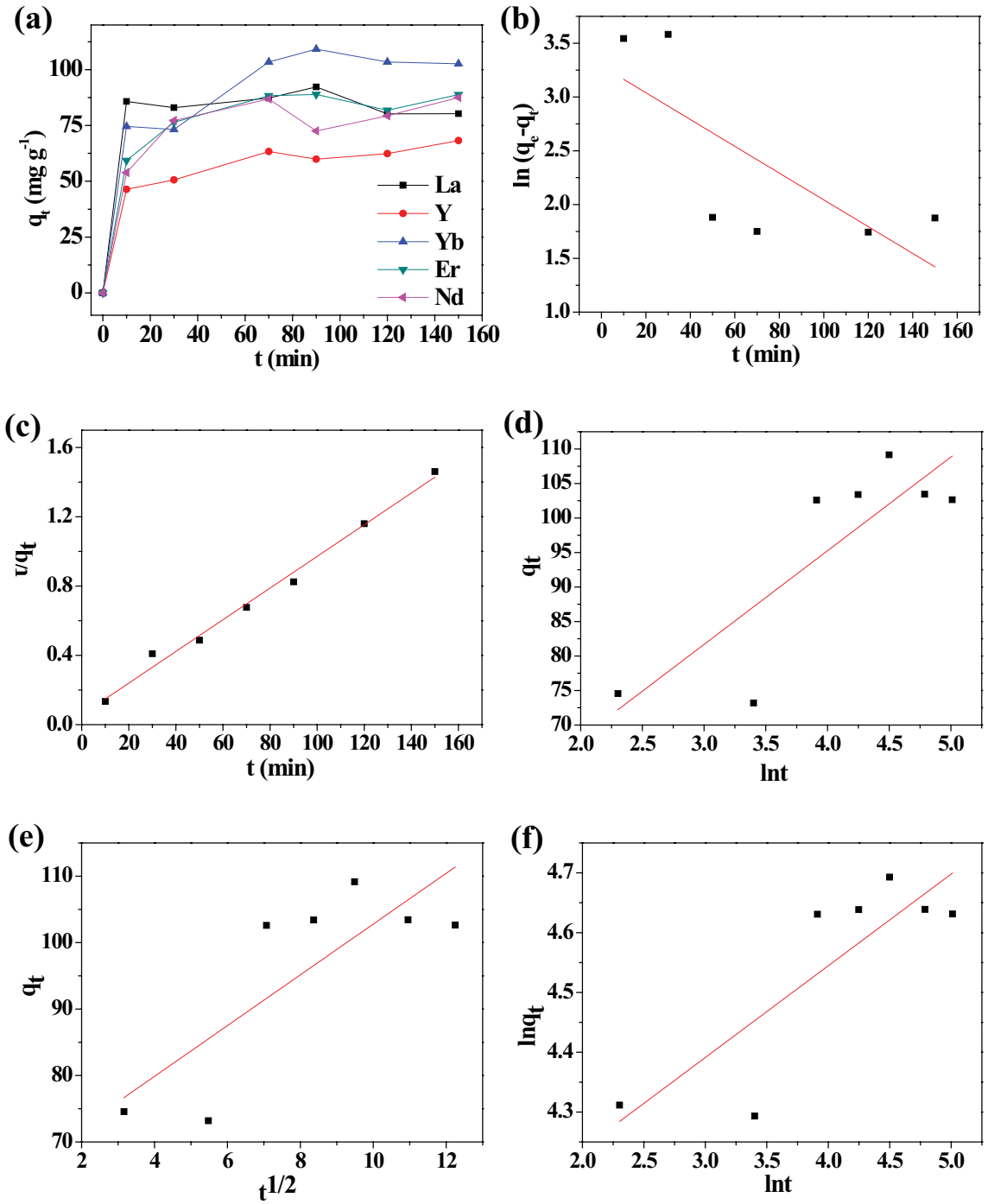

Fig. 4. Adsorption kinetics for REE^{3+} onto GO-CCl_2 composite: (a) effects of contact time on the adsorption of La^{3+}, Yb^{3+}, Y^{3+}, Er^{3+} and Nd^{3+} onto GO-CCl_2 at 308 K. The kinetics data of GO-CCl_2 composite for Yb^{3+} fitted to various models: (b) pseudo-first-order kinetic model, (c) pseudo-second-order kinetic model, (d) Elovich model, (e) Weber–Morris model and (f) Bangham model.

$$q_t = \frac{1}{\beta}(\ln \alpha\beta) + \frac{1}{\beta}\ln t \quad (3)$$

$$q_t = k_{ip} t^{1/2} + C \quad (4)$$

$$\ln q_t = \ln k_b + \frac{1}{m}\ln t \quad (5)$$

where k_1 (1 min^{-1}) and k_2 (g mg^{-1} min^{-1}) are the rate constants of pseudo-first-order kinetic model and pseudo-second-order kinetic model; q_e (mg g^{-1}) and q_t (mg g^{-1}) are the adsorption quantity at equilibrium and time t; α (mmol g^{-1} min^{-1}) is the initial adsorption rate; β (g mmol^{-1}) is desorption constant; k_{ip} (mg g^{-1} min$^{-1/2}$) is the intraparticle diffusion constant; while m and k_b are the relevant constants of Bangham model.

The kinetic parameters of the five models were calculated (Table 1). It is obvious that the adsorption of Yb^{3+} onto GO-CCl_2 composite fitted better to pseudo-second-order kinetic model with a much higher coefficient of determination (R^2), indicating that the adsorption process was mainly determined by a chemical interaction. Chemical reactions between the electron-rich chlorine-containing/oxygen-containing groups and the unoccupied orbitals of REE^{3+} were significant as the rate-controlling steps in the adsorption [46].

3.3. Adsorption isotherms

In addition, the adsorption isotherms were also studied to reveal the effects of temperature on the adsorption behaviors (Fig. 5a). The initial concentrations of Yb^{3+} solutions were in the range of 10–80 mg L^{-1}, and the adsorption temperatures were set as 298, 308 and 318 K. The adsorption capacities of GO-CCl_2 composite for Yb^{3+} increased with an increase in contact temperature. The adsorption data were fitted by Langmuir (Eq. (6)), Freundlich (Eq. (7)) and Temkin (Eq. (8)) isotherm models which could be expressed as follows:

$$\frac{C_e}{q_e} = \frac{1}{K_L q_m} + \frac{C_e}{q_m} \tag{6}$$

$$\ln q_e = \ln K_F + \frac{1}{n}\ln C_e \tag{7}$$

$$q_e = \frac{RT}{b_T}\ln C_e + \frac{RT}{b_T}\ln A_T \tag{8}$$

Table 1
Kinetic parameters for the adsorption of Yb^{3+}

Pseudo-first-order model			Pseudo-second-order model			Elovich model			Weber–Morris model		Bangham model		
k_1	q_e	R^2	k_2	q_e	R^2	α	β	R^2	k_{ip}	R^2	M	k_b	R^2
0.0125	26.80	0.4339	0.0015	109.3	0.9889	278.0	0.0737	0.6511	3.8199	0.5743	6.5190	50.96	0.6529

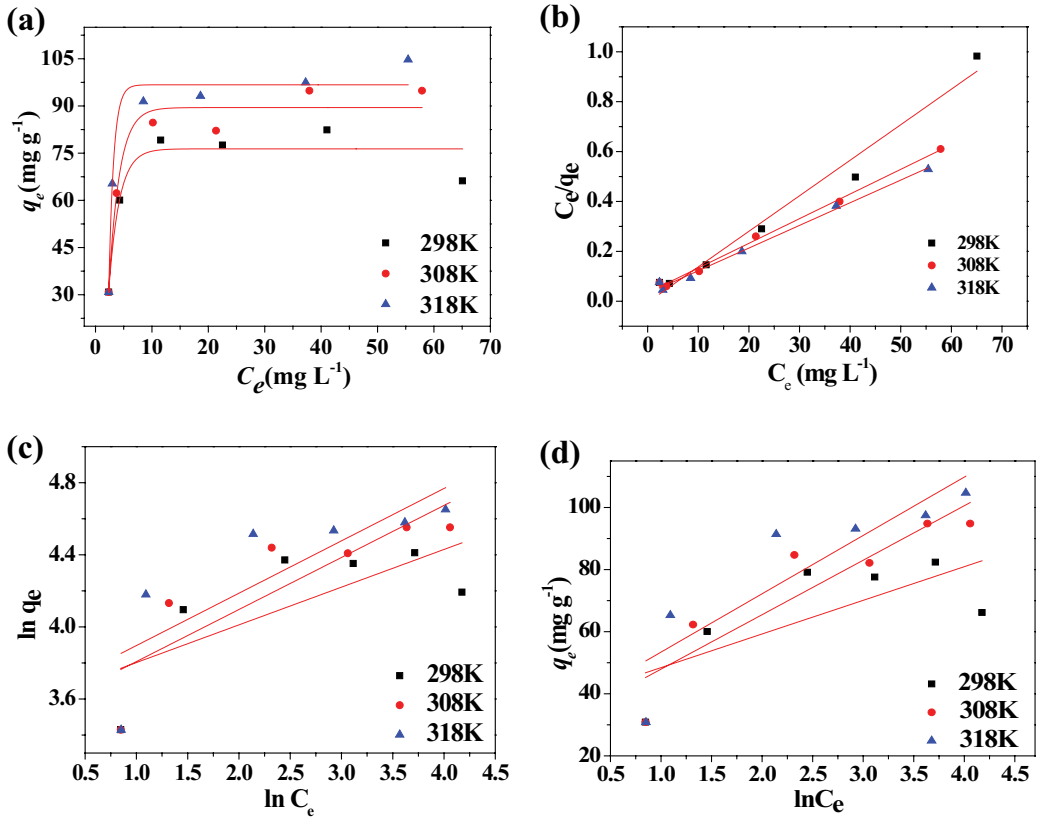

Fig. 5. (a) Adsorption capacities of GO-CCl_2 for Yb^{3+} at 298, 308 and 318 K; Yb^{3+} adsorption isotherms of GO-CCl_2 composite: (b) Langmuir isotherm model, (c) Freundlich isotherm model and (d) Temkin isotherm model.

where q_e (mg g^{-1}) and q_m (mg g^{-1}) are the equilibrium adsorption capacity and maximum adsorption capacity; C_e (mg L^{-1}) is the equilibrium concentration of metal ions in solutions; K_L and K_F are Langmuir constant and physical constant of Freundlich isotherm, respectively; n is an empirical constant relating to adsorption intensity; while b_T is a physical quantity which is related with adsorption heat.

The isotherm parameters for the adsorption of Yb^{3+} by GO-CCl_2 composite were fitted (Table 2). A higher correlation coefficient values (R^2) represented that the adsorption of Yb^{3+} onto GO-CCl_2 composite fitted better by Langmuir model than Freundlich and Temkin models (Figs. 5b–d), indicating that the chemical monolayer adsorption occurred on the as-prepared material. The maximum adsorption capacities of GO-CCl_2 composite are about 70.225, 101.11 and 110.13 mg g^{-1} at 298, 308 and 318 K, respectively.

3.4. Thermodynamic study

The entropy changes ($\Delta S°$), enthalpy changes ($\Delta H°$) and standard free energy changes ($\Delta G°$) were calculated according to the thermodynamic equations (Eqs. (9)–(11)):

$$K_d = \frac{(C_0 - C_e)}{C_e} \times \frac{V}{m} \tag{9}$$

$$\ln K_d = -\frac{\Delta H°}{RT} + \frac{\Delta S°}{R} \tag{10}$$

$$\Delta G° = \Delta H° - T\Delta S° \tag{11}$$

where T (K) and K_d (L mg^{-1}) represent the absolute temperature and standard thermodynamic equilibrium constant; C_0 (mg L^{-1}) and C_e (mg L^{-1}) are the initial concentration and equilibrium concentration of Yb^{3+} solution, respectively; R (8.314 J mol^{-1} K^{-1}) means the gas constant.

The thermodynamic parameters for the adsorption of Yb^{3+} by GO-CCl_2 composite were analyzed (Fig. 6; Table 3). From the positive values of $\Delta H°$ and $\Delta S°$, and negative value of $\Delta G°$, it can be deduced that the adsorption of Yb^{3+} by GO-CCl_2 composite was a spontaneous and endothermic reaction. When the magnitude of $\Delta H°$ is 8–16 kJ mol^{-1}, the adsorption type can be explained by chemical adsorption. Therefore, we could infer that the adsorption of Yb^{3+} onto GO-CCl_2 composite can be defined as a chemical adsorption process ($\Delta H°$ = 17.78 kJ mol^{-1}) [47]. And the thermodynamic data were consistent with those obtained from adsorption isotherm and kinetic studies.

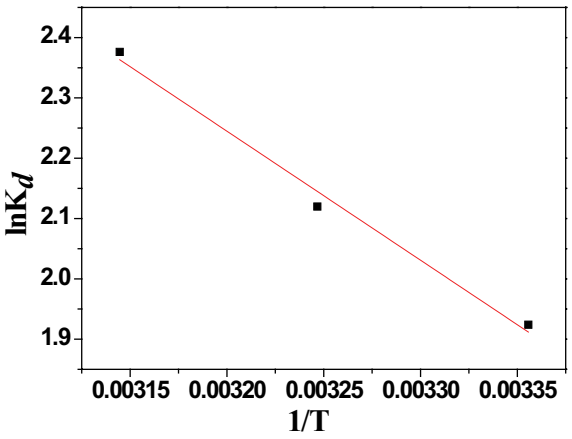

Fig. 6. Fitted thermodynamic curve of adsorption of Yb^{3+} onto GO-CCl_2 composite.

Table 3
Thermodynamic parameters for the adsorption of Yb^{3+} onto GO-CCl_2 composite

T (K)	$\Delta H°$ (kJ mol^{-1})	$\Delta S°$ (J mol^{-1} K^{-1})	$\Delta G°$ (kJ mol^{-1})
298			–4.74
308	17.78	75.57	–5.50
318			–6.25

3.5. Adsorption mechanism

Normally, the oxygen-containing groups can interact with metal ions, making GO possess higher adsorption efficiency than that of reduced GO [48]. The metals including transition or main group species could also interact with halogen through coordination bond [49]. The introduced halogen bonds (–CCl_2) on to GO can provide additional interactions for REE^{3+}, and GO-CCl_2 possessed higher adsorption capacity than that of GO. Meanwhile, the adsorption capacities of GO-CX_2 (X = F, Cl, Br or I) for REE^{3+} could be regulated by changing the halogen species because the strength and the possibilities of GO-CX_2 M (M is metal) would change.

3.6. Evaluation of adsorption capacities in real samples

GO-CCl_2 composite was applied to adsorb La^{3+}, Y^{3+}, Yb^{3+}, Er^{3+} and Nd^{3+} in spring water, Xiangjiang river water, Yudai river waiter and tap water, respectively. No or little REE^{3+} ions

Table 2
Isotherm parameters for the adsorption of Yb^{3+}

T (K)	Langmuir model			Freundlich model			Temkin model		
	b	q_m	R^2	K_f	$1/n$	R^2	b_T	A_T	R^2
298	–3.1786	70.225	0.972	36.336	0.2096	0.424	228.60	3.468	0.417
308	0.2867	101.11	0.995	33.746	0.2888	0.666	145.90	1.730	0.786
318	0.2879	110.13	0.993	36.812	0.2905	0.567	140.66	1.842	0.728

Table 4
Analytical recoveries for the determination of La^{3+}, Y^{3+}, Yb^{3+}, Er^{3+} and Nd^{3+} in water samples (sorbent = 10 mg, volume = 20 mL, added concentration = 20 mg L^{-1})

Samples	La^{3+} (%)	Y^{3+} (%)	Yb^{3+} (%)	Er^{3+} (%)	Nd^{3+} (%)
Spring water	95.28	70.52	88.41	88.69	89.82
Xiangjiang river water	98.74	85.59	91.26	92.55	96.13
Yudai river water	99.15	91.72	89.96	92.32	95.99
Tap water	100.00	98.48	88.31	90.91	94.95

existed in these four kinds of real water samples. Recovery experiments were carried out by adding standard samples into the real water samples (Table 4). Most of the recoveries were calculated to be more than 90%, confirming the excellent adsorption performance of GO-CCl_2 composite for REE^{3+} from complicated real water samples.

4. Conclusion

In this work, a facile hydrothermal method was successfully conducted to obtain a novel GO-CCl_2 nanocomposite. The relevant characterizations such as FT-IR, Raman spectroscopy, TGA and FE-SEM were carried out to reveal the structural features and surface groups of GO-CCl_2 nanocomposite. The adsorption kinetics, isotherms and thermodynamics of GO-CCl_2 nanocomposite for Yb^{3+} were investigated in detail. The adsorption performances of GO-CCl_2 composite for REE^{3+} in real samples including spring water, Xiangjiang River water, Yudai River water and tap water were also studied, and the as-prepared material showed satisfactory adsorption capacity in these complicated water systems. In summary, the proposed GO-CCl_2 composite can be used in the adsorption, removal and enrichment of REE ions from aqueous solutions.

Acknowledgments

The authors are grateful to the financial support from National Natural Science Foundation of China (Nos. 51674292, 21471163 and 51574118), Provincial Natural Science Foundation of Hunan (No. 2016JJ1023) and Hunan Provincial Science and Technology Plan Project, China (No. 2018TP1003).

References

[1] D.L. Ramasamy, V. Puhakka, E. Repo, S. Ben Hammouda, M. Sillanpää, Two-stage selective recovery process of scandium from the group of rare earth elements in aqueous systems using activated carbon and silica composites: dual applications by tailoring the ligand grafting approach, Chem. Eng. J., 341 (2018) 351–360.
[2] J. Roosen, K. Binnemans, Adsorption and chromatographic separation of rare earths with EDTA- and DTPA-functionalized chitosan biopolymers, J. Mater. Chem. A, 2 (2013) 1530–1540.
[3] W. Chen, L. Wang, M. Zhuo, Y. Liu, Y. Wang, Y. Li, Facile and highly efficient removal of trace Gd(III) by adsorption of colloidal graphene oxide suspensions sealed in dialysis bag, J. Hazard. Mater., 279 (2014) 546–553.
[4] X. Xu, J. Zou, X.-R. Zhao, X.-Y. Jiang, F.-P. Jiao, J.-G. Yu, Q. Liu, J. Teng, Facile assembly of three-dimensional cylindrical egg white embedded graphene oxide composite with good reusability for aqueous adsorption of rare earth elements, Colloids Surf., A, 570 (2019) 127–140.
[5] Y.F. Xu, Z.B. Liu, X.L. Zhang, Y. Wang, J.G. Tian, Y. Huang, Y.F. Ma, X.Y. Zhang, Y.S. Chen, A graphene hybrid material covalently functionalized with porphyrin: synthesis and optical limiting property, Adv. Mater., 21 (2009) 1275–1279.
[6] M.R. Yaftian, M. Burgard, C.B. Dieleman, D. Matt, Rare-earth metal-ion separation using a supported liquid membrane mediated by a narrow rim phosphorylated calix[4]arene, J. Membr. Sci., 144 (1998) 57–64.
[7] J.P. Faris, J.W. Warton, Anion exchange resin separation of the rare earths, yttrium, and scandium in nitric acid-methanol mixtures, Anal. Chem., 34 (1962) 1077–1080.
[8] R. Chi, Z. Zhou, Z. Xu, Y. Hu, G. Zhu, S. Xu, Solution-chemistry analysis of ammonium bicarbonate consumption in rare-earth-element precipitation, Metall. Mater. Trans. B, 34 (2003) 611–617.
[9] K.C. Kemp, H. Seema, M. Saleh, N.H. Le, K. Mahesh, V. Chandra, K.S. Kim, Environmental applications using graphene composites: water remediation and gas adsorption, Nanoscale, 5 (2013) 3149–3171.
[10] Y. Takahashi, X. Châtellier, K.H. Hattori, K. Kato, D. Fortin, Adsorption of rare earth elements onto bacterial cell walls and its implication for REE sorption onto natural microbial mats, Chem. Geol., 219 (2005) 53–67.
[11] H.M.H. Gad, N.S. Awwad, Factors affecting on the sorption/desorption of Eu (III) using activated carbon, Sep. Sci. Technol., 42 (2007) 3657–3680.
[12] O.I.M. Ali, H.H. Osman, S.A. Sayed, M.E.H. Shalabi, The removal of some rare earth elements from their aqueous solutions on by-pass cement dust (BCD), J. Hazard. Mater., 195 (2011) 62–67.
[13] T. Yoshida, T. Ozaki, T. Ohnuki, A.J. Francis, Adsorption of rare earth elements by γ-Al_2O_3 and *Pseudomonas fluorescens* cells in the presence of desferrioxamine B: implication of siderophores for the Ce anomaly, Chem. Geol., 212 (2004) 239–246.
[14] X. Xu, X.Y. Jiang, F.P. Jiao, X.Q. Chen, J.G. Yu, Tunable assembly of porous three-dimensional graphene oxide-corn zein composites with strong mechanical properties for adsorption of rare earth elements, J. Taiwan Inst. Chem. Eng., 85 (2018) 106–114.
[15] S. Wang, H. Sun, H.M. Ang, M.O. Tadé, Adsorptive remediation of environmental pollutants using novel graphene-based nanomaterials, Chem. Eng. J., 226 (2013) 336–347.
[16] K.S. Novoselov, A.K. Geim, S.V. Morozov, D. Jiang, Y. Zhang, S.V. Dubonos, I.V. Grigorieva, A.A. Firsov, Electric field effect in atomically thin carbon films, Science, 306 (2004) 666–669.
[17] M. Soylak, D. Acar, E. Yilmaz, S.A. El-Khodary, M. Morsy, M. Ibrahim, Magnetic graphene oxide as an efficient adsorbent for the separation and preconcentration of Cu(II), Pb(II), and Cd(II) from environmental samples, J. AOAC Int., 100 (2017) 1544–1550.
[18] J. Zou, L. Huang, X. Jiang, F. Jiao, J. Yu, Electrochemical behaviors and determination of rifampicin on graphene nanoplatelets modified glassy carbon electrode in sulfuric acid solution, Desal. Wat. Treat., 120 (2018) 272–281.
[19] J. Zou, G. Zhao, J. Teng, Q. Liu, X. Jiang, F. Jiao, J. Yu, Highly sensitive detection of bisphenol A in real water samples based on in-situ assembled graphene nanoplatelets and gold nanoparticles composite, Microchem. J., 145 (2019) 693–702.

[20] J. Zou, X.Q. Chen, G.Q. Zhao, X.Y. Jiang, F.P. Jiao, J.G. Yu, A novel electrochemical chiral interface based on the synergistic effect of polysaccharides for the recognition of tyrosine enantiomers, Talanta, 195 (2019) 628–637.
[21] D. Li, R.B. Kaner, Graphene-based materials, Science, 320 (2008) 1170–1171.
[22] D.A. Dikin, S. Stankovich, E.J. Zimney, R.D. Piner, G.H. Dommett, G. Evmenenko, S.T. Nguyen, R.S. Ruoff, Preparation and characterization of graphene oxide paper, Nature, 448 (2007) 457–460.
[23] B.Z. Jang, A. Zhamu, Processing of nanographene platelets (NGPs) and NGP nanocomposites: a review, J. Mater. Sci., 43 (2008) 5092–5101.
[24] S. Park, R.S. Ruoff, Chemical methods for the production of graphenes, Nat. Nanotechnol., 4 (2009) 217.
[25] M. Khan, E. Yilmaz, B. Sevinc, E. Sahmetlioglu, J. Shah, M.R. Jan, M. Soylak, Preparation and characterization of magnetic allylamine modified graphene oxide-poly (vinyl acetate-co-divinylbenzene) nanocomposite for vortex assisted magnetic solid phase extraction of some metal ions, Talanta, 146 (2016) 130–137.
[26] B. Yue, L. Yu, F. Jiao, X. Jiang, J. Yu, The fabrication of pentaerythritol pillared graphene oxide composite and its adsorption performance towards metal ions from aqueous solutions, Desal. Wat. Treat., 102 (2018) 124–133
[27] F. Zhou, X. Feng, J. Yu, X. Jiang, High performance of 3D porous graphene/lignin/sodium alginate composite for adsorption of Cd(II) and Pb(II), Environ. Sci. Pollut. Res., 25 (2018) 15651–15661.
[28] C. Liang, X. Feng, J. Yu, X. Jiang, Facile one-step hydrothermal syntheses of graphene oxide-MnO_2 composite and their application in removing heavy metal ions, Micro Nano Lett., 13 (2018) 1179–1184.
[29] C. Liang, X. Feng, J. Yu, X. Jiang, Graphene oxide/Mg-Fe layered double hydroxide composites for highly efficient removal of heavy metal ions from aqueous solution, Desal. Wat. Treat., 132 (2018) 109–119.
[30] D. Li, M.B. Müller, S. Gilje, R.B. Kaner, G.G. Wallace, Processable aqueous dispersion of graphene nanosheets, Nat. Nanotechnol., 3 (2008) 101–105.
[31] J. Kim, L.J. Cote, F. Kim, W. Yuan, K.R. Shull, J. Huang, Graphene oxide sheets at interfaces, J. Am. Chem. Soc., 132 (2010) 8180–8186.
[32] X. Zeng, J. Yu, D. Fu, H. Zhang, J. Teng, Wear characteristics of hybrid aluminum-matrix composites reinforced with well-dispersed reduced graphene oxide nanosheets and silicon carbide particulates, Vacuum, 155 (2018) 364–375.
[33] X.R. Zhao, X. Xua, X.Y. Jiang, J. Teng, J.G. Yu, Facile fabrication of three-dimensional and recyclable graphene oxide-melamine composites with high removal efficiency, Desal. Wat. Treat., 148 (2019) 188–194.
[34] Y. Sun, D. Shao, C. Chen, S. Yang, X. Wang, Highly efficient enrichment of radionuclides on graphene oxide-supported polyaniline, Environ. Sci. Technol., 47 (2013) 9904–9910.
[35] V. Chandra, J. Park, Y. Chun, J.W. Lee, I.C. Hwang, K.S. Kim, Water-dispersible magnetite-reduced graphene oxide composites for arsenic removal, ACS Nano, 4 (2010) 3979–3986.
[36] J. Yang, B. Yue, J. Teng, X. Xu, X. Zhao, X. Jiang, J. Yu, F. Zhou, Aqueous metal ions adsorption by poly(ethylene glycol) modified graphene oxide: surface area and surface chemistry effects, Desal. Wat. Treat., 138 (2019) 147–158.
[37] Z.N. Huang, Z. Jiao, J. Teng, Q. Liu, M.M. Yuan, F.P. Jiao, X.Y. Jiang, J.G. Yu, A novel electrochemical sensor based on self-assembled platinum nanochains - Multi-walled carbon nanotubes-graphene nanoparticles composite for simultaneous determination of dopamine and ascorbic acid, Ecotoxicol. Environ. Saf., 172 (2019) 167–175.
[38] R.P. Medina, E.T. Nadres, F.C. Ballesteros, D.F. Rodrigues, Incorporation of graphene oxide into a chitosan–poly(acrylic acid) porous polymer nanocomposite for enhanced lead adsorption, Environ. Sci. Nano, 3 (2016) 638–646.
[39] S. Wang, X. Li, Y. Liu, C. Zhang, X. Tan, G. Zeng, B. Song, L. Jiang, Nitrogen-containing amino compounds functionalized graphene oxide: Synthesis, characterization and application for the removal of pollutants from wastewater: a review, J. Hazard. Mater., 342 (2017) 177–191.
[40] N. Zhou, Y. Wang, L. Huang, J. Yu, H. Chen, J. Tang, F. Xu, X. Lu, M.-e. Zhong, Z. Zhou, In situ modification provided by a novel wet pyrolysis system to enhance surface properties of biochar for lead immobilization, Colloids Surf., A, 570 (2019) 39–47.
[41] X.Z. Feng, Y.K. Zhang, C.Y. Liang, J.G. Yu, X.Y. Jiang, GO/PDDA/Fe_3O_4 nanocomposites used for instantaneous Cr(VI) removal and a reliable direct filtration-adsorption application, Desal. Wat. Treat., 153 (2019) 145–156.
[42] X.R. Zhao, X. Xu, J. Teng, N. Zhou, Z. Zhou, X.Y. Jiang, F.P. Jiao, J.G. Yu, Three-dimensional porous graphene oxide-maize amylopectin composites with controllable pore-sizes and good adsorption-desorption properties: facile fabrication and reutilization, and the adsorption mechanism, Ecotoxicol. Environ. Saf., 176 (2019) 11–19.
[43] D.C. Marcano, D.V. Kosynkin, J.M. Berlin, A. Sinitskii, Z. Sun, A. Slesarev, L.B. Alemany, W. Lu, J.M. Tour, Improved synthesis of graphene oxide, ACS Nano, 4 (2010) 4806–4814.
[44] X. Xu, J. Zou, J. Teng, Q. Liu, X.Y. Jiang, F.P. Jiao, J.G. Yu, X.Q. Chen, Novel high-gluten flour physically cross-linked graphene oxide composites: hydrothermal fabrication and adsorption properties for rare earth ions, Ecotoxicol. Environ. Saf., 166 (2018) 1–10.
[45] X. Zeng, J. Teng, J.G. Yu, A.S. Tan, D.F. Fu, H. Zhang, Fabrication of homogeneously dispersed graphene/Al composites by solution mixing and powder metallurgy, Int. J. Miner. Metall. Mater., 25 (2018) 102–109.
[46] Y.S. Ho, G. McKay, Pseudo-second-order model for sorption processes, Process Biochem., 34 (1999) 451–465.
[47] D. Angin, Utilization of activated carbon produced from fruit juice industry solid waste for the adsorption of Yellow 18 from aqueous solutions, Bioresour. Technol., 168 (2014) 259–266.
[48] Z. Wang, X. Li, H. Liang, J. Ning, Z. Zhou, G. Li, Equilibrium, kinetics and mechanism of Au^{3+}, Pd^{2+} and Ag^{+} ions adsorption from aqueous solutions by graphene oxide functionalized persimmon tannin, Mater. Sci. Eng. C, 79 (2017) 227–236.
[49] L. Brammer, G. Mínguez Espallargas, S. Libri, Combining metals with halogen bonds, CrystEngComm, 10 (2008) 1712–1727.